ACS APPLIED MATERIALS & INTERFACES

Research Article

www.acsami.org

Unusual Air Filters with Ultrahigh Efficiency and Antibacterial Functionality Enabled by ZnO Nanorods

Zhaoxiang Zhong,[†] Zhe Xu,[†] Ting Sheng,[†] Jianfeng Yao,[‡] Weihong Xing,*[,†] and Yong Wang*[,†]

[†]State Key Laboratory of Materials-Oriented Chemical Engineering, National Engineering Research Center for Specialized Separation Membranes, Nanjing Tech University, Nanjing 210009, China

[‡]College of Chemical Engineering, Nanjing Forestry University, Nanjing 210037, China

Supporting Information

ABSTRACT: Porous membranes/filters that can remove airborne fine particulates, for example, PM2.5, with high efficiency at low energy consumption are of significant interest. Herein, we report on the fabrication of a new class of unusual superior air filters with ultrahigh efficiency and an interesting antibacterial functionality. We use atomic layer deposition (ALD) to uniformly seed ZnO on the surface of expanded polytetrafluoroethylene (ePTFE) matrix, and then synthesize well-aligned ZnO nanorods with tunable widths and lengths from the seeds under hydrothermal conditions. The presence of ZnO nanorods reduces the effective pore sizes of the ePTFE filters at little expense of energy consumption. As a consequence, the filters exhibit exceptional dust removal efficiencies greater than 99.9999% with much lower energy consumption than conventional filters. Significantly, the presence of ZnO nanorods strongly inhibits the propagation of both Gram positive and negative bacteria on the filters. Therefore, the functionalized filters can potentially overcome the inherent limitation in the trade-off effect and imply their superiority for controlling indoor air quality.

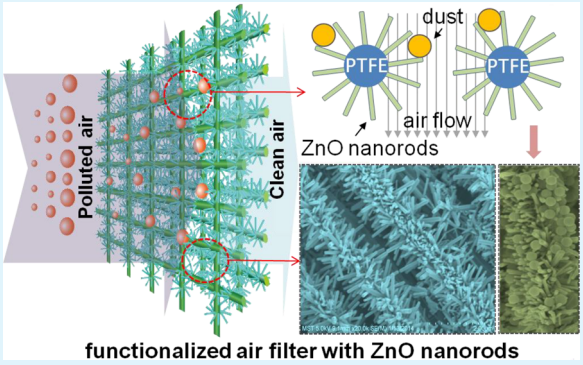

KEYWORDS: *PM2.5, antibacterial coating, atomic layer deposition, membranes, ZnO nanorods*

1. INTRODUCTION

Airborne fine particulates raise severe health and safety issues as they can be inhaled and may also cause explosions. It is vital to improve the indoor air quality by controlling these particulates under a certain concentration both in industry and in our daily life.[1−3] Filtration is a common method for fine particulate removal and air cleaning, which involves capturing particulates through mechanisms of direct interception, inertial impaction, and diffusion.[4] However, commonly used filters suffer from a frustrated trade-off effect between the particulate removal efficiency and the air permeability characterized by pressure drop across the filters. High particulate removal efficiency is usually achieved at the expense of high pressure drop and correspondingly high energy consumption. Moreover, filters in long-term use are prone to be contaminated by microorganisms, which not only causes additional health concerns but also further increases the pressure drop with the continuous propagation of bacteria covering the filter surface and penetrating into the filters.[5] Therefore, much effort is required to design advanced filters that combine the advantages of high particulate removal efficiency, low pressure drop, and bacteria-inhibiting functionality.

There are two types of air filters commonly used.[6] The first one is in the form of fibrous layers consisting of randomly stacked one-dimensional (1D) nanostructures such as carbon nanotubes,[7−9] inorganic nanowires,[10,11] and polymer nanofibers.[12] The second one is made up of three-dimensionally interconnected porous networks including foam-like graphene,[13] spongy ceramics,[14] and expanded polytetrafluoroethylene (ePTFE).[15] The fibrous layers of 1D nanostructures have a large surface-area-to-volume ratio that can increase the contact area between particulates and fibers, and thus improve the particulate removal efficiencies. In addition, when the diameter of the fibers is comparable to the mean free path of the "air molecules" (~66 nm), the gas velocity is nonzero at the fiber surface as "slip" flow occurs.[16] The slip flow makes the airflow near the fiber surface larger than that of nonslip flow, which causes more particles to travel near the fiber and then results in higher diffusion and impaction efficiencies. The three-dimensional (3D) spongy-like air filter has high porosities and the fine meshes exhibit little resistance to airflow, which typically results in low pressure drops. However, the penetration of fine particles into the highly porous matrix lowers the removal efficiencies and progressively clogs filter pores.[15,17] In this work, we combine the advantages of these two filters by growing 1D ZnO nanorods (NRs) on the 3D porous networks of ePTFE, and obtain a new form of air filters with a hierarchal fibrous structure exhibiting ultrahigh removal

Received: July 26, 2015
Accepted: September 11, 2015
Published: September 11, 2015

DOI: 10.1021/acsami.5b06810
ACS Appl. Mater. Interfaces 2015, 7, 21538−21544

efficiency and extremely low pressure drop. Additionally, the filters possess very desirable antibacterial functionality because of the conjunction of ZnO NRs on the network of ePTFE.

2. EXPERIMENTAL SECTION

Materials. Porous ePTFE filters in the form of round chips (Φ25 mm × 0.65 mm) were purchased from Sartorius (Germany) and used as received. The ALD reactants were diethylzinc ($Zn(C_2H_5)_2$, DEZ, Aladdin) and deionized H_2O, which were used as the zinc and oxygen source, respectively. N_2 with high purity (99.99%) was used as the carrier and the purging gas. Zinc nitrate hydrate ($Zn(NO_3)_2{\cdot}6H_2O$) and hexamethylenetetramine (HMTA, $C_6H_{12}N_4$) were purchased from Shanghai Lingfeng Chemical Co. All chemical reagents were of analytical grade and were used as received without further purification. Monodispersed SiO_2 particles with a diameter of 0.30 and 1.2 μm were synthesized by the Stoeber method, and their SEM images were shown in Figure S1.

Deposition of ZnO Seeding Layers. ZnO ALD was carried out in a hot-wall ALD reactor (S100, Cambridge NanoTech). ePTFE filters were positioned in the ALD chamber preheated to 130 °C with both sides directly exposed to the nitrogen stream. The ALD reaction was initiated when the vacuum in the chamber reached 1 Torr. The precursor DEZ was heated to 40 °C while water was heated to 60 °C. These two precursor vapors were alternately delivered into the reaction chamber, and the exposure mode was used to allow the precursors to thoroughly diffuse and adsorb into the samples. A typical ALD cycle included (i) DEZ pulse for 1 s; (ii) exposure for 10 s; (iii) purge for 35 s; (iv) H_2O pulse for 0.1 s; (v) exposure for 10 s; and (vi) purge for 35 s. The filters were deposited for 300 cycles at 130 °C under a steady nitrogen flow rate of 20 sccm.

As for the dip-coating method, ePTFE filters were immersed in a 5 mM ethanolic solution of zinc acetate dihydrate. Subsequently, the zinc acetate films on the ePTFE substrates were annealed at 250 °C in air for 1 h.

Hydrothermal Growth of ZnO Nanorods. ZnO-ALD ePTFE substrates were immersed in a 35 mL aqueous solution with equimolar (5 mM) zinc nitrate and HMTA in an autoclave. The reaction was conducted at 90 °C for 3 h. Subsequently, the sample was washed repeatedly with deionized water and then dried naturally in air.

Characterizations. SEM images were taken using a field emission scanning electron microscope (FESEM, HitachiS-4800) equipped with an energy dispersive X-ray detector (EDX). Some ZnO seeds and nanorods were removed from the filters using a sharp blade and examined with transmission electron microscopy (TEM, JEOL 3010 Japan) and SAED. X-ray diffraction (XRD) patterns were obtained on a Bruker D8-Advance X-ray diffractometer with the scanning speed and step size of 2° min^{-1} and 0.02°, respectively. The adsorption properties were determined by nitrogen sorption at 77 K using a Micromeritics ASAP 2020 volumetric sorptometer. The surface area was calculated by using the Brunauer–Emmett–Teller (BET) method. The gas bubble pressure (GBP) method was used to measure the pore sizes of the filters. All of the samples were immersed in alcohol for 2 h under reduced pressure. The flow rate and transmembrane pressure of nitrogen across the membrane were recorded to estimate the pore size.

Filtration Tests. The experimental setup used for testing the performance of filters is shown in Figure S2. The air cylinder provided clean, dry air with stable flow to the system at room temperature. The air flow was first split into two ways. One stream that contained a glass fluidized bed ash feeder was designed to feed SiO_2 particles into the gas stream, while the other that had no ash feeder served as the dilution air for control. The two streams then merged, delivering gas flow with particle concentration of 1.00 ± 0.1 g m^{-3}, and passed through the filter at room temperature. The particle concentrations upstream and downstream of the filters were measured in situ with an aerosol dust monitoring instrument (DustTrak II 8530, U.S.). The detection limit for the monitoring instrument is 0.001 mg/m^3. Two pressure gauges were used for measuring the pressure drop of the test filter media. The gas flow rate was controlled at 4 cm s^{-1} by control valves. After filtration, the filters then go through a cleaning cycle to release the deposited particles during which the filters are pulsed from the permeate side to the feed side with compressed air from the pulse gas tank. The pressure of compressed air was 20 kPa, and the pulse width was 0.2 s.

The removal efficiency (R) of aerosols is determined by the following equation:

$$R = \left(1 - \frac{C_p}{C_f}\right) \times 100\% \quad (1)$$

where C_f is the feed concentration and C_p is the permeate concentration.

Antibacterial Performance Tests. The antimicrobial efficiency of the filter medium was examined against Gram negative bacterium (*Escherichia coli* (ATCC11303), *E. coli*) and Gram positive bacterium (*Staphylococcus aureus* (ATCC 6538), *S. aureus*). *E. coli* and *S. aureus* were purchased from Shanghai Seebio Biotech, Inc. The antibacterial performances were determined as follows:[18] Both microbial species were grown in broth solutions (Luria–Bertani broth for *E. coli*, and tryptic soy broth for *S. aureus*) for 24 h at 37 °C. The bacteria were harvested by centrifugation, washed with phosphate buffered saline (PBS), and then resuspended in PBS to the density of 10^4~10^5 colony forming units per milliliter (CFU mL^{-1}). 100 μL of the freshly prepared bacterial suspensions was placed onto the surfaces of filters samples (3.0 ± 0.1 cm^2) under room lighting conditions. After 15 min, the sample was transferred into 10 mL of sterilized PBS and vortexed for 2 min to transfer the adherent bacteria into PBS. The solution was then diluted serially, and 100 μL of each diluent was placed onto agar plates (Luria–Bertani agar for *E. coli*, and tryptic soy agar for *S. aureus*). Colony forming units on the agar plates were counted under an optical microscope after incubation at 37 °C for 24 h. Each test was repeated three times. The reported data were the average value of three parallel runs.

The sterilization rate was determined by using the following formula:

$$\text{sterilization rate} = \frac{A - B}{A} \times 100\% \quad (2)$$

where A is the number of living bacterium in the control sample, and B is the number of living bacterium in the testing sample.

3. RESULTS AND DISCUSSION

Microstructure Characterizations and Separation Performances Test of the Filters. The schematic for the preparation process and the morphologies of the filter at different stages are shown in Figure 1. The preparation of the filters contains two simple steps: seeding of ZnO nanoparticles on the ePTFE networks and hydrothermal growth of ZnO NRs on the seeding layer. The hydrothermal growth of aligned ZnO NRs on a substrate usually requires a thin and uniform ZnO layer as the seeding material. Pristine ePTFE filters manufactured by a stretching process are highly porous and exhibit a net-like structure composed of interconnected and smooth nanofibrils. We first tried to produce the seeding layer on the ePTFE filter by the conventional dip-coating seeding process but failed to obtain a uniform coverage of ZnO on the surface (Figure S3). We then turned to atomic layer deposition (ALD) to produce the seeding layer as ALD has been demonstrated to be a very effective and well-controlled technique to produce thin coating layers on various substrates including porous materials.[19−23] Moreover, it has been recently reported that metal oxides including ZnO can be easily deposited on both dense PTFE films and porous membranes despite the extremely inert nature of PTFE.[19,21,23,24] As is clearly shown by SEM images, after ALD treatment, the original smooth surface of the nanofibrils in ePTFE is covered by densely arranged nanoparticles. Energy dispersive X-ray

DOI: 10.1021/acsami.5b06810
ACS Appl. Mater. Interfaces 2015, 7, 21538−21544

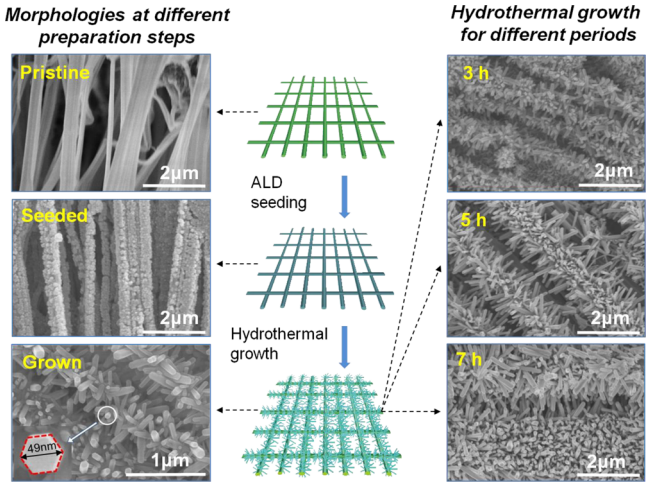

Figure 1. Schematic of the preparation process of the ZnO-functionalized ePTFE filters and the SEM images of the filters at different stages. The inset shows the magnified top-view SEM image of an individual ZnO NR prepared with a hydrothermal growth period for 3 h.

spectroscopy (EDX) analysis reveals the relatively uniform distribution of Zn throughout the surface of the filter and the approximately 1:1 atomic ratio of zinc and oxygen (Figure S4), indicating that ZnO was successfully deposited on the ePTFE substrate. ZnO was deposited on the ePTFE surface as isolated nanoparticles rather than continuous films. This is because ePTFE has a very inert surface lack of active groups, and the ALD deposition proceeds in the mode of subsurface growth in which precursors are diffused into the near surface regions of the ePTFE substrates.[19,21,23,24]

The ZnO-ALD ePTFE was then subjected to hydrothermal treatment in an aqueous solution of zinc nitrate and hexamethylenetetramine for the growth of ZnO NRs. Densely packed ZnO NRs appear on the fibrils of the ePTFE support after hydrothermal treatment for a period of 3 h. The ZnO NRs are aligned roughly perpendicularly to the axis of the fibrils, yielding a hierarchical "NRs-on-nanofibrils" morphology. We note that the adhesion of ZnO NRs grown on ePTFE filter is reasonably strong as the majority of the NRs remains on the filter after an ultrasonication oscillation treatment at 150 W for 10 min (Figure S5). Such an oscillation treatment results in only a very slight weight loss (~0.11%), confirming that few NRs have been detached from the ePTFE support. The top-view SEM image of an individual NR is shown as the inset in Figure 1, indicating a hexagonal crystalline shape. X-ray diffraction was employed to analyze the crystalline phase of the ZnO seeds and also the hydrothermally grown ZnO NRs. Both ZnO nanostructures exhibit a hexagonal wurtzite structure, although the ZnO seeds show much weaker diffraction intensity as compared to the ZnO NRs (Figure S6). Characterizations by the high-resolution transmission electron microscopy and electron diffraction (Figure S7) reveal that the NRs are single crystalline with a [0001] growth direction and are preferentially oriented in the *c*-axis direction, which is consistent with hydrothermally grown ZnO NRs reported in other works.[25−28]

Longer hydrothermal treatment leads to increase in length and width of the ZnO NRs. The average width of the NRs

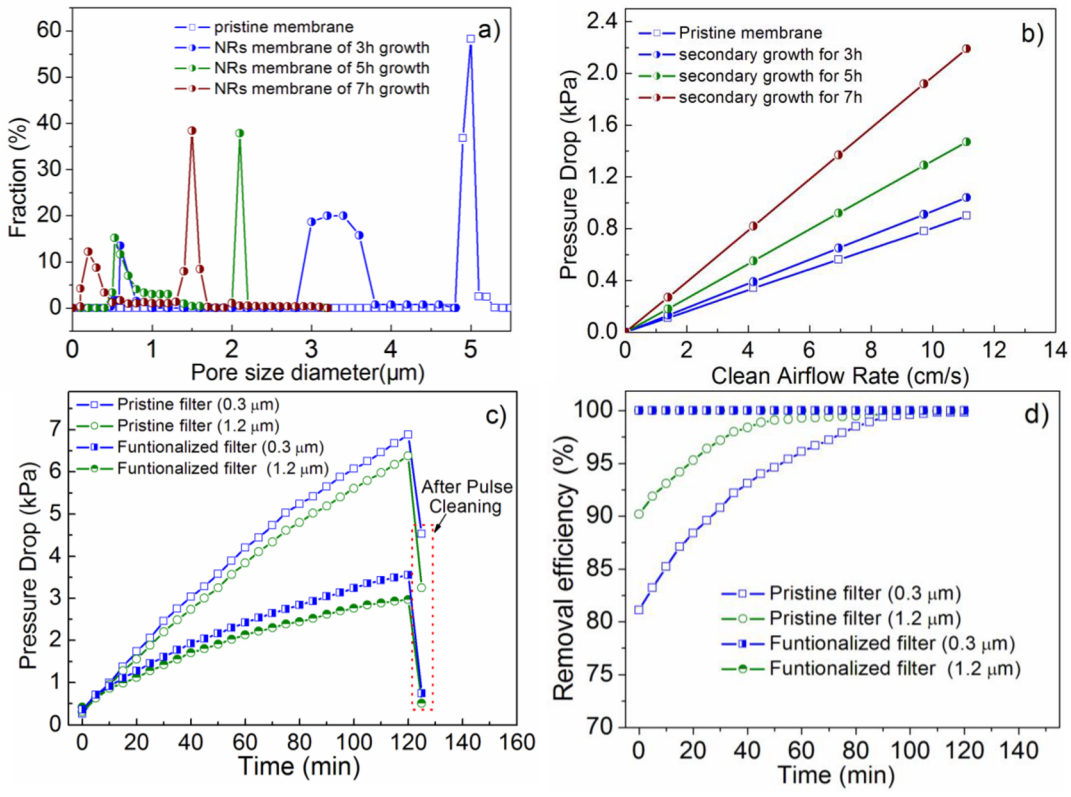

Figure 2. Pore size distribution of functionalized filters obtained at different periods of hydrothermal treatment (a), the pressure drop across the corresponding filters (b), the change of pressure drops (c), and particulate removal efficiencies (d) of the pristine and functionalized filters (with a hydrothermal treatment for 3 h) with the operation time in the filtration of airborne SiO_2 particles with diameters of 1.2 and 0.3 μm.

DOI: 10.1021/acsami.5b06810
ACS Appl. Mater. Interfaces 2015, 7, 21538−21544

treatment is 37 nm after a hydrothermal treatment for a period of 3 h, which increases to 67 and 82 nm after 5 and 7 h, respectively (Figure S8). The growing NRs reduce the free spaces between the nanofibrils that define the pores in the ePTFE filter for air transmission. We tested the effective pore sizes of these filters subjected to different periods of hydrothermal growth using the gas bubbling pressure method. For the pristine ePTFE filter, the peak pore size is centered around ~5 μm. In contrast, the ZnO NRs-functionalized filters prepared at different hydrothermal treatment all show a bimodal pore size distribution (Figure 2a). The filter prepared with a hydrothermal growth for 3 h exhibits pores with sizes in the ranges of 1.5−4 and 0.1−0.6 μm, respectively. The bigger pores arise from the free spaces between the nanofibrils decorated with aligned NRs, whereas the small pores represent the spaces between adjacent ZnO NRs. The size of the aforementioned pores reduces with increasing periods of hydrothermal treatment due to the increasing width and length of the ZnO NRs.

Clean air permeability tests were first conducted on the pristine and functionalized ePTFE filters. As shown in Figure 2b, the pressure drops across the pristine filter, and functionalized filters prepared with the hydrothermal treatment for 3, 5, and 7 h are around 0.9, 1.04, 1.47, and 2.19 kPa at a flow rate of 11 cm s^{-1}, respectively. It is clear that the growth of ZnO NRs on ePTFE supports increases the filtration resistance due to the reducing effective pore sizes. To balance between the pressure drop and the removal efficiency, the functionalized filters prepared with a moderate hydrothermal growth period of 3 h were selected for further permeability and dust capture tests. As can be seen from Figure 2c, in the filtration of airborne dusts with different sizes the pristine filters has a lower initial pressure drop than the functionalized filters, which is due to the above-mentioned reduction of the average pore size of the ePTFE filters after the growth of ZnO NRs. However, with the extension of operation time, the pressure drop of the pristine ePTFE filter increases much faster than that of the functionalized filters and eventually reaches a much higher pressure drop. The change of pressure drops with operation time implies that the pristine ePTFE filter is severely clogged while the functionalized filter largely maintains a good porous structure with continuous filtration under dust load. The pressure drop of the filter filtrating SiO_2 particles with the diameter of 0.3 μm is higher than that for SiO_2 particles with the diameter of 1.2 μm. This is because smaller particles more easily penetrate the filter pores, increasing the filtrating resistance; meanwhile, the dust layer formed by smaller particles results in a high specific cake resistance.[29]

Figure 2d shows the SiO_2 particulates removal efficiencies of pristine and functionalized filters. For the pristine filter, the initial removal efficiencies are 81.1% for 0.3 μm particulates and 90.2% for 1.20 μm particles, respectively. The removal efficiencies increase with filtration time as a filter cake builds up, which acts as an additional filtration barrier. Impressively, for the functionalized filter, the removal efficiencies are greater than 99.9999% for both particulates. It is notable that the functionalized filters achieve high removal efficiencies, and maintain low pressure drops. These behaviors indicate the excellent surface filtration characteristics of the filters functionalized with ZnO NRs, which directly lead to lower energy consumption and significant cost savings throughout the life cycle.

Moreover, the functionalized filters display a much better ability to be cleaned after use. We used pulsed gas to clean the used filters as pulse cleaning is a conventional physical method to reduce fouling and pressure drop. As is shown in Figure 2c, after pulse cleaning with compressed gas at 20 kPa, the pressure drop of the functionalized filter decreases immediately to a very low level (~0.5 kPa), while that of the pristine filter maintains at a high level (~3.2 kPa) due to the retaining of particles inside the pores. It is clear that the functionalized filter can be regenerated more effectively, requiring less frequent cleaning and providing longer filter life.

Particle Capture Mechanisms by the Filters. According to the classical filtration theory, sieving, inertial impaction, interception, and diffusion are the most important filtration mechanisms in air filtration.[7,16] The particle retention efficiency is typically determined by more than one of these mechanisms, and the predominant one depends mainly on the specific particle size. The particles with diameters in the range of 0.2−2 μm are difficult to remove from air by filtration,[14,30] especially those with a diameter of ~0.3 μm, which is called the most penetrating particle size (MPPS) giving the minimum efficiency. In this study, two monodispersed SiO_2 particulates with diameters of 0.30 and 1.2 μm, respectively, were used to model the airborne dusts. The predominant capture mechanism for the pristine ePTFE filter to 0.30 μm particulates was considered to be the diffusion effect, a mechanism often used for particulates of size less than 0.5 μm. As shown in Figure 3a, small particulates move randomly onto the ePTFE fibrils in the filter during collisions with other particulates and gas molecules, and some of them adhere to the surface of the fibrils. However, if the adhesion force is not strong enough, these particulates may slip around the fibrils and move away from the fibrils.[31] Consequently, the particulates penetrate deep into the filter as revealed by SEM examinations. It was reported that nanofibers with a large surface-area-to-volume ratio can increase the probability of aerosol deposition on the fiber surface by diffusion, thus improving the filter efficiency.[32] One conventional method to increase the surface-area-to-volume ratio is to fabricate filters with narrower fibers.[33] Here, we demonstrated a new strategy to increase the surface-area-to-volume ratio by forming additional fibrous structures with very small diameters down to less than 100 nm (ZnO NRs) on the original fibrils in the ePTFE filter (Figure 3b). With the presence of the ZnO NRs on the filter, the surface area of the filter increases to 7.4 m^2 g^{-1} from 4.3 m^2 g^{-1} for the pristine filter (Figure S9), and the apparent density increases to 0.37 g cm^{-3} from 0.21 g cm^{-3}. As a result, we can roughly estimate that the surface-area-to-volume ratio of the functionalized filter increases to 2.74×10^6 m^2 m^{-3} from 0.90×10^6 m^2 m^{-3} for the pristine filter. With higher surface-area-to-volume ratios, the functionalized filters have larger interaction areas to capture particles through the adhesion between particles and ZnO NRs, which increases the probability of aerosol deposition on the fiber surface by diffusion. In general, due to the very high surface-area-to-volume ratio and consequently high surface adhesion, small particles can be easily trapped on the functionalized filter surface, and hence the filtration efficiency can be improved.

When the particle size is larger than 0.5 μm, the inertial impaction and interception effects become pronounced.[32] Impaction occurs when the inertia of the particle carries it into the filter fibril, even though the gas stream flows around the fibril. Impaction will occur at greater chance for larger particles. In the interception mechanism, even if the particle is

DOI: 10.1021/acsami.5b06810
ACS Appl. Mater. Interfaces 2015, 7, 21538−21544

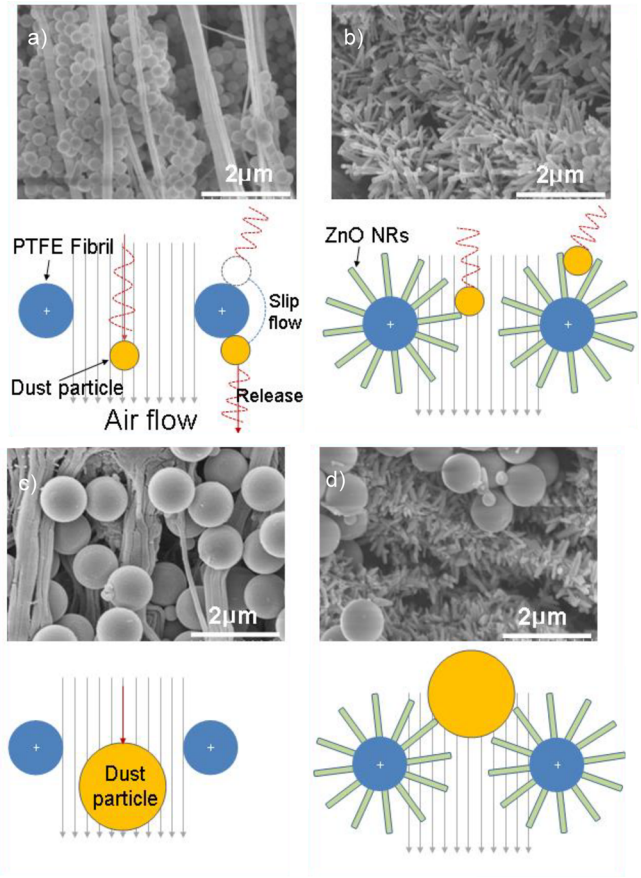

Figure 3. SEM images and the corresponding schematic of the particle capture mechanism of the pristine ePTFE filter filtrating 0.3 μm particles (a), the functionalized ePTFE filter filtrating 0.3 μm particles (b), the pristine ePTFE filter filtrating 1.2 μm particles (c), and the functionalized ePTFE filter filtrating 1.2 μm particles (d). Particles with sizes of 0.3 and 1.2 μm represent the nanosized and microsized particles, respectively.

light enough to follow the streamlines of the gas flow around the fibril, the particle is still large enough and will eventually come into contact with the fibril as it passes. However, as the 1.2 μm SiO_2 particles are smaller than the pristine filter pore size, there are still some particles entering and passing through the filter networks (Figure 3c). The growth of ZnO NRs narrows the space between filter fibrils, resulting in sieving filtration. The particles do not enter deep into the filter but are retained on the filter surface (Figure 3d). Air filtration occurs in two ways: surface filtration and depth filtration. The most significant implication of using surface versus depth filtration is the location of captured particles. In surface filtration, the particles accumulate in a thin layer right at the surface of the filter, whereas in depth filtration they accumulate inside pores throughout some depth. This fouling resistance could be calculated on the basis of experimental data.[34] The relative percentages of resistance for different membranes are shown in Table 1.

For a fluid moving with a slow steady velocity, the pressure drop (ΔP) through the filter and the flow rate (ν) are related through the Darcy law.[35]

$$\Delta P = \nu \cdot \eta \cdot R \tag{3}$$

where ν is flow rate, ΔP is pressure drop, R_t is total filtration resistance, and η is dynamic viscosity of the fluid. It is assumed

Table 1. Resistance Percentages of the Pristine and Functionalized Filters after Filtration

filter	particle size (μm)	$\Delta R_0/\Delta R_t$ (%)	$\Delta R_i/\Delta R_t$ (%)	$\Delta R_c/\Delta R_t$ (%)
pristine filter	0.3	4.78	71.7	23.52
	1.2	5.16	56.13	38.71
functionalized filter	0.3	5.76	5.44	88.80
	1.2	7.0	1.30	91.70

that total filtration resistance is the sum of intrinsic membrane resistance (R_0), cake resistance by cake layer formed on membrane surface (R_c), and fouling resistance caused by inside pore blocking (R_i); that is, the R_t is defined as $R_t = R_0 + R_i + R_c$.

Those resistances can be calculated from experimental data using the following equations:

$$R_0 = \frac{\Delta P_0}{\eta \cdot \nu} \tag{4}$$

$$R_i = \frac{\Delta P_i}{\eta \cdot \nu} - R_0 \tag{5}$$

$$R_c = \frac{\Delta P_t}{\eta \cdot \nu} - R_0 - R_i \tag{6}$$

where ΔP_0 is the initial pressure drop before filtration, ΔP_t is the pressure drop of membrane after filtration, and ΔP_i is the pressure drop after removing cake layer. The flow rate is controlled constantly, and the cake layer was removed by a suitable brush. For the filters functionalized with ZnO NRs, the fouling resistance analysis (Table 1) shows that the formation of the dust layer on the filter surface is the dominant fouling mechanism and the blocking resistance is insignificant (<6% of the total resistance), while for the pristine ePTFE filter, blocking is the main fouling mechanism (>50% of the total resistance). Therefore, the growth of ZnO NRs changes the filtration mechanisms from depth filtration to surface filtration without introducing significant increase in flow resistance.

The quality factor ($QF = -\ln(1 - E)/\Delta P$, where E is the particulate removal efficiency and ΔP is the pressure drop) is usually used to compare the filtration performance of different filters. A better filter should possess a higher filtration efficiency and lower pressure drop, which corresponds to a higher QF value.[7] As can be seen from Table 2, the functionalized ePTFE filter prepared in this work demonstrates the highest filtration efficiency, and its final pressure drop is also among the lowest values, and consequently it displays the highest QF among the commercialized and reported filters prepared from different materials.

Antibacterial Activity of the Functionalized Filters. ZnO NRs have been demonstrated to exhibit excellent antibacterial properties and have been used as antimicrobial coatings.[36−39] We expect that the filters functionalized with ZnO NRs may also exhibit antibacterial property. To evaluate the antibacterial effect of the filters with and without ZnO NRs, the filters were exposed to both Gram negative bacterium (*E. coli*) and Gram positive bacterium (*S. aureus*) solutions. The counts for *E. coli* and *S. aureus* were 9210 and 24 160, respectively (Table S1) in the bacterium solution incubated from the solution exposed to the pristine filter (Figure 4a,b), which indicates that the pristine ePTFE filter does not possess an evident antimicrobial effect within the testing period. Therefore, once attached on the filter, the microorganism

DOI: 10.1021/acsami.5b06810
ACS Appl. Mater. Interfaces 2015, 7, 21538−21544

Table 2. Performance Comparison between Functionalized Filters Prepared in This Work and Other Filters

filter media	filtration efficiency for d_p = 0.3 μm (%)	pressure drop before filtration (kPa)	pressure drop after filtration (kPa)	QF for d_p = 0.3 μm (kPa^{-1})	sterilization rates (%)
commercial ePTFE filter of this work	96.1120	0.31	4.20	0.77	0
functionalized filter of this work	99.9999	0.36	2.42	3.80	99.0
commercial cellulose filter II[7]	98.76	2.11	2.11	2.65	
multiwalled carbon nanotubes filter[7]	99.9994	0.22	5.42	2.75	

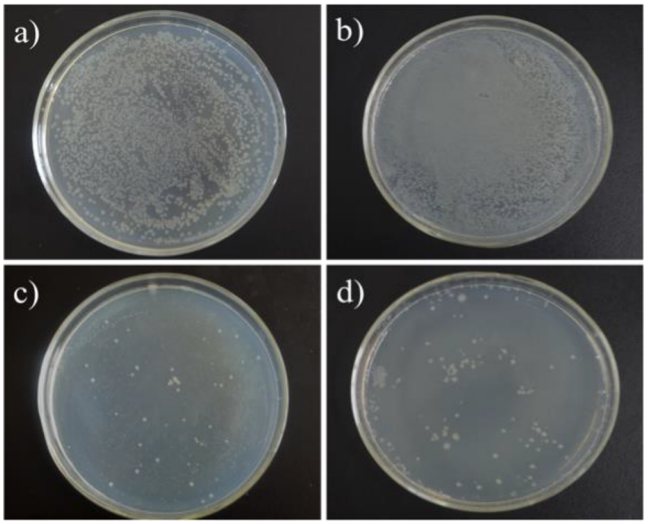

Figure 4. Photographs of the diluted *E. coli* (a) and *S. aureus* (b) solutions from pristine ePTFE filter, and the diluted *E. coli* (c) and *S. aureus* (d) solutions from functionalized ePTFE.

species will readily propagate on the filter, causing microorganism build-ups and consequent health risks and reduced capability of air cleaning. However, the counts of bacterial colonies in suspension exposed to functionalized filters were only 51 and 123, respectively (Figure 4c,d). The sterilization rates against *E. coli* and *S. aureus* for the functionalized filter were both higher than 99.0%, demonstrating excellent antibacterial property. There are two possible mechanisms for the antimicrobial effect of ZnO NRs under visible light. One is that the hydroxyl radicals (•OH) and/or hydrogen peroxide (H_2O_2) generated by the photocatalysis effect of the ZnO NRs effectively inhibit the bacterial growth by penetrating the cell wall of the bacteria,[36,37,40,41] and the other is that the slow release of Zn^{2+} ions arising from partial dissolution of ZnO in a moist environment leads to the rupture of the bacterial cell wall.[42] The high antibacterial activity of the filter functionalized with ZnO NRs will provide highly desirable benefits in terms of rapidly inactivating captured microorganisms, preventing the clogging of the filter caused by the microbial growth and avoiding the secondary bacterial contamination of the cleaned filter. Apart from the common particulate filtration, this new antibacterial filter is exceptionally suitable for sterile filtration of fermentation feed air. Furthermore, ZnO NRs are commonly used to decompose organic pollutants under light irradiation;[43] the filter may also be useful in cleaning polluted air containing volatile organic compounds (VOCs).

4. CONCLUSIONS

In summary, unusual filters with high efficiency, low energy consumption, and antibacterial functionality are produced in this work by growing aligned ZnO NRs onto the fibrous matrix of ePTFE filters. The ZnO NRs are grown on the seeding layer of ZnO particulates deposited on ePTFE using the ALD technique. The densely packed ZnO NRs notably change the pore structure of the pristine ePTFE filter at little expense of the flow resistance. The filters functionalized with ZnO NRs are exceptional in several ways including high air filtration efficiencies (>99.9999% to the most penetrating particles), low pressure drops (about 40% less than the filters without ZnO NRs), easy pulse cleaning of surface-filtered particles, and interestingly a high antibacterial activity (>99.0% sterilization rates against both Gram-positive and -negative bacteria). Such high-efficient, antibacterial air filters are expected to find broad applications in industrial gas purification devices and indoor air cleaning systems.

■ ASSOCIATED CONTENT

Supporting Information

The Supporting Information is available free of charge on the ACS Publications website at DOI: 10.1021/acsami.5b06810.

Additional characterization results on the functionalized filters and ZnO nanorods (PDF)

■ AUTHOR INFORMATION

Corresponding Authors

*E-mail: xingwhong@163.com.
*E-mail: yongwang@njtech.edu.cn.

Notes

The authors declare no competing financial interest.

■ ACKNOWLEDGMENTS

Financial support was provided by the National Natural Science Foundation of China (21125629, 21276124, 21450585), Jiangsu Province Scientific Supporting Project (BE2014717).

■ REFERENCES

(1) Hughes, V. Public Health Where There's Smoke. *Nature* **2012**, *489*, S18−S20.
(2) Wang, Q. China's Citizens Must Act to Save Their Environment. *Nature* **2013**, *497*, 159−159.
(3) Zhang, Q.; He, K. B.; Huo, H. Cleaning China's Air. *Nature* **2012**, *484*, 161−162.
(4) Denny, F.; Permana, E.; Scott, J.; Wang, J.; Pui, D. Y. H.; Amal, R. Integrated Photocatalytic Filtration Array for Indoor Air Quality Control. *Environ. Sci. Technol.* **2010**, *44*, 5558−5563.
(5) Jung, J. H.; Hwang, G. B.; Lee, J. E.; Bae, G. N. Preparation of Airborne Ag/CNT Hybrid Nanoparticles Using an Aerosol Process and Their Application to Antimicrobial Air Filtration. *Langmuir* **2011**, *27*, 10256−10264.
(6) Kaur, S.; Gopal, R.; Ng, W. J.; Ramakrishna, S.; Matsuura, T. Next-Generation Fibrous Media for Water Treatment. *MRS Bull.* **2008**, *33*, 21−26.

DOI: 10.1021/acsami.5b06810
ACS Appl. Mater. Interfaces 2015, 7, 21538−21544

(7) Viswanathan, G.; Kane, D. B.; Lipowicz, P. J. High Efficiency Fine Particulate Filtration Using Carbon Nanotube Coatings. *Adv. Mater.* **2004**, *16*, 2045−2049.
(8) Srivastava, A.; Srivastava, O. N.; Talapatra, S.; Vajtai, R.; Ajayan, P. M. Carbon Nanotube Filters. *Nat. Mater.* **2004**, *3*, 610−614.
(9) Brady-Estevez, A. S.; Kang, S.; Elimelech, M. A Single-Walled-Carbon-Nanotube Filter for Removal of Viral and Bacterial Pathogens. *Small* **2008**, *4*, 481−484.
(10) Ke, X. B.; Zhu, H. Y.; Gao, X. P.; Liu, J. W.; Zheng, Z. F. High-Performance Ceramic Membranes With a Separation Layer of Metal Oxide Nanofibers. *Adv. Mater.* **2007**, *19*, 4325−4325.
(11) Liang, H. W.; Wang, L.; Chen, P. Y.; Lin, H. T.; Chen, L. F.; He, D. A.; Yu, S. H. Carbonaceous Nanofiber Membranes for Selective Filtration and Separation of Nanoparticles. *Adv. Mater.* **2010**, *22*, 4691−4696.
(12) Liu, C.; Hsu, P. C.; Lee, H. W.; Ye, M.; Zheng, G. Y.; Liu, N. A.; Li, W. Y.; Cui, Y. Transparent Air Filter for High-Efficiency PM2.5 Capture. *Nat. Commun.* **2015**, *6*, 1−9.
(13) Chen, Z. P.; Ren, W. C.; Gao, L. B.; Liu, B. L.; Pei, S. F.; Cheng, H. M. Three-Dimensional Flexible and Conductive Interconnected Graphene Networks Grown by Chemical Vapour Deposition. *Nat. Mater.* **2011**, *10*, 424−428.
(14) de Freitas, N. L.; Goncalves, J. A. S.; Innocentini, M. D. M.; Coury, J. R. Development of a Double-Layered Ceramic Filter for Aerosol Filtration at High-Temperatures: the Filter Collection Efficiency. *J. Hazard. Mater.* **2006**, *136*, 747−756.
(15) Yoon, K.; Hsiao, B. S.; Chu, B. Functional Nanofibers for Environmental Applications. *J. Mater. Chem.* **2008**, *18*, 5326−5334.
(16) Li, P.; Wang, C. Y.; Zhang, Y. Y.; Wei, F. Air Filtration in the Free Molecular Flow Regime: a Review of High-Efficiency Particulate Air Filters Based on Carbon Nanotubes. *Small* **2014**, *10*, 4543−4561.
(17) Barg, S.; Innocentini, M. D. M.; Meloni, R. V.; Chacon, W. S.; Wang, H. L.; Koch, D.; Grathwohl, G. Physical and High-Temperature Permeation Features of Double-Layered Cellular Filtering Membranes Prepared via Freeze Casting of Emulsified Powder Suspensions. *J. Membr. Sci.* **2011**, *383*, 35−43.
(18) Zhang, L. F.; Luo, J. E.; Menkhaus, T. J.; Varadaraju, H.; Sun, Y. Y.; Fong, H. Antimicrobial Nano-Fibrous Membranes Developed From Electrospun Polyacrylonitrile Nanofibers. *J. Membr. Sci.* **2011**, *369*, 499−505.
(19) Lee, S. M.; Ischenko, V.; Pippel, E.; Masic, A.; Moutanabbir, O.; Fratzl, P.; Knez, M. An Alternative Route towards Metal-Polymer Hybrid Materials Prepared by Vapor-Phase Processing. *Adv. Funct. Mater.* **2011**, *21*, 3047−3055.
(20) Knez, M.; Niesch, K.; Niinisto, L. Synthesis and Surface Engineering of Complex Nanostructures by Atomic Layer Deposition. *Adv. Mater.* **2007**, *19*, 3425−3438.
(21) Wilson, C. A.; Grubbs, R. K.; George, S. M. Nucleation and Growth During Al_2O_3 Atomic Layer Deposition on Polymers. *Chem. Mater.* **2005**, *17*, 5625−5634.
(22) Kemell, M.; Farm, E.; Ritala, M.; Leskela, M. Surface Modification of Thermoplastics by Atomic Layer Deposition of Al_2O_3 And TiO_2 Thin Films. *Eur. Polym. J.* **2008**, *44*, 3564−3570.
(23) Xu, Q.; Yang, Y.; Wang, X. Z.; Wang, Z. H.; Jin, W. Q.; Huang, J.; Wang, Y. Atomic Layer Deposition of Alumina on Porous Polytetrafluoroethylene Membranes for Enhanced Hydrophilicity and Separation Performances. *J. Membr. Sci.* **2012**, *415*, 435−443.
(24) Parsons, G. N.; Atanasov, S. E.; Dandley, E. C.; Devine, C. K.; Gong, B.; Jur, J. S.; Lee, K.; Oldham, C. J.; Peng, Q.; Spagnola, J. C.; Williams, P. S. Mechanisms and Reactions during Atomic Layer Deposition on Polymers. *Coord. Chem. Rev.* **2013**, *257*, 3323−3331.
(25) Greene, L. E.; Yuhas, B. D.; Law, M.; Zitoun, D.; Yang, P. D. Solution-Grown Zinc Oxide Nanowires. *Inorg. Chem.* **2006**, *45*, 7535−7543.
(26) Liu, B.; Zeng, H. C. Hydrothermal Synthesis of ZnO Nanorods in the Diameter Regime of 50 nm. *J. Am. Chem. Soc.* **2003**, *125*, 4430−4431.
(27) Greene, L. E.; Law, M.; Tan, D. H.; Montano, M.; Goldberger, J.; Somorjai, G.; Yang, P. D. General Route to Vertical ZnO Nanowire Arrays Using Textured ZnO Seeds. *Nano Lett.* **2005**, *5*, 1231−1236.
(28) Dai, H.; Zhou, Y.; Liu, Q.; Li, Z.; Bao, C.; Yu, T.; Zhou, Z. Controllable Growth of Dendritic ZnO Nanowire Arrays on a Stainless Steel Mesh Towards the Fabrication of Large Area, Flexible Dye-Sensitized Solar Cells. *Nanoscale* **2012**, *4*, 5454−5460.
(29) Altmann, J.; Ripperger, S. Particle Deposition and Layer Formation at the Crossflow Microfiltration. *J. Membr. Sci.* **1997**, *124*, 119−128.
(30) Darcovich, K.; Jonasson, K. A.; Capes, C. E. Developments in the Control of Fine Particulate Air Emissions. *Adv. Powder Technol.* **1997**, *8*, 179−215.
(31) Sambaer, W.; Zatloukal, M.; Kimmer, D. 3D Air Filtration Modeling for Nanofiber Based Filters in the Ultrafine Particle Size Range. *Chem. Eng. Sci.* **2012**, *82*, 299−311.
(32) Li, H. W.; Wu, C. Y.; Tepper, F.; Lee, J. H.; Lee, C. N. Removal and Retention of Viral Aerosols by a Novel Alumina Nanofiber Filter. *J. Aerosol Sci.* **2009**, *40*, 65−71.
(33) Ma, Z. W.; Kotaki, M.; Ramakrishna, S. Electrospun Cellulose Nanofiber as Affinity Membrane. *J. Membr. Sci.* **2005**, *265*, 115−123.
(34) Zhong, Z. X.; Li, W. X.; Xing, W. H.; Xu, N. P. Crossflow Filtration of Nanosized Catalysts Suspension Using Ceramic Membranes. *Sep. Purif. Technol.* **2011**, *76*, 223−230.
(35) Miguel, A. F. Effect of Air Humidity on the Evolution of Permeability and Performance of a Fibrous Filter During Loading with Hygroscopic and Non-Hygroscopic Particles. *J. Aerosol Sci.* **2003**, *34*, 783−799.
(36) Wang, X. L.; Yang, F.; Yang, W.; Yang, X. R. A Study on the Antibacterial Activity of One-Dimensional ZnO Nanowire Arrays: Effects of the Orientation and Plane Surface. *Chem. Commun.* **2007**, 4419−4421.
(37) Applerot, G.; Lipovsky, A.; Dror, R.; Perkas, N.; Nitzan, Y.; Lubart, R.; Gedanken, A. Enhanced Antibacterial Activity of Nanocrystalline ZnO Due to Increased ROS-Mediated Cell Injury. *Adv. Funct. Mater.* **2009**, *19*, 842−852.
(38) Brayner, R.; Ferrari-Iliou, R.; Brivois, N.; Djediat, S.; Benedetti, M. F.; Fievet, F. Toxicological Impact Studies Based on Escherichia Coli Bacteria in Ultrafine ZnO Nanoparticles Colloidal Medium. *Nano Lett.* **2006**, *6*, 866−870.
(39) Tang, C.; Spencer, M. J. S.; Barnard, A. S. Activity of ZnO Polar Surfaces: an Insight from Surface Energies. *Phys. Chem. Chem. Phys.* **2014**, *16*, 22139−22144.
(40) Ghule, K.; Ghule, A. V.; Chen, B. J.; Ling, Y. C. Preparation and Characterization of ZnO Nanoparticles Coated Paper and its Antibacterial Activity Study. *Green Chem.* **2006**, *8*, 1034−1041.
(41) Okyay, T. O.; Bala, R. K.; Nguyen, H. N.; Atalay, R.; Bayam, Y.; Rodrigues, D. F. Antibacterial Properties and Mechanisms of Toxicity of Sonochemically Grown ZnO Nanorods. *RSC Adv.* **2015**, *5*, 2568−2575.
(42) Han, J.; Qiu, W.; Gao, W. Potential Dissolution and Photo-Dissolution of ZnO Thin Films. *J. Hazard. Mater.* **2010**, *178*, 115−122.
(43) Zhang, X. Y.; Qin, J. Q.; Xue, Y. N.; Yu, P. F.; Zhang, B.; Wang, L. M.; Liu, R. P. Effect of Aspect Ratio and Surface Defects on the Photocatalytic Activity of Zno Nanorods. *Sci. Rep.* **2014**, *4*, 1−8.

DOI: 10.1021/acsami.5b06810
ACS Appl. Mater. Interfaces 2015, 7, 21538−21544